Influence of edge plasma turbulence on the low-threshold parametric decay instability at ECRH

P V Tretinnikov, A Yu Popov, E Z Gusakov, S Heuraux

▶ **To cite this version:**

P V Tretinnikov, A Yu Popov, E Z Gusakov, S Heuraux. Influence of edge plasma turbulence on the low-threshold parametric decay instability at ECRH. Physics of Plasmas, 2023, 30 (2), pp.022111. 10.1063/5.0132560 . hal-04003802

HAL Id: hal-04003802

https://hal.univ-lorraine.fr/hal-04003802

Submitted on 24 Feb 2023

HAL is a multi-disciplinary open access archive for the deposit and dissemination of scientific research documents, whether they are published or not. The documents may come from teaching and research institutions in France or abroad, or from public or private research centers.

L'archive ouverte pluridisciplinaire **HAL**, est destinée au dépôt et à la diffusion de documents scientifiques de niveau recherche, publiés ou non, émanant des établissements d'enseignement et de recherche français ou étrangers, des laboratoires publics ou privés.

Influence of edge plasma turbulence on the low-threshold parametric decay instability at ECRH

P V Tretinnikov[1,2,a)], A Yu Popov[1], E Z Gusakov[1], S Heuraux[2]
1 Ioffe Institute, 194021 Saint-Petersburg, Russia
2 Institut Jean Lamour, 50400 Nancy, France
a) Author to whom correspondence should be addressed: tretinnikov@mail.ioffe.ru

Abstract: the saturation level of the two-Upper-Hybrid-plasmon (UH) low-threshold parametric decay instability (PDI) depend on the pump wave beam width. The edge plasma turbulence may lead to drastic distortion of the pump beam, thus generating PDI characteristics changes. Numerical evaluations of the PDI process are provided in this work for different turbulence scenarios. The average PDI characteristics are evaluated and compared to the simulation results for the pump beam unperturbed by the edge plasma turbulence. It is shown that up to the intermediate turbulence level the PDI characteristics are only gently modified. But at high edge turbulence level, which can happen in tokamaks, the threshold increases and the growth rate reduces. It is important to note that the anomalous absorption keeps a little reduction value, whatever the edge turbulence regimes.

1 Introduction

The electron cyclotron resonance heating (ECRH) is a popular method to produce and heat a fusion relevant plasma in magnetic confinement devices [1]. It is based on the theoretical predictions of localized microwave energy deposition and of suppression of nonlinear phenomena which can accompany the microwave propagation and damping. However, during the last decade various anomalous effects (anomalous microwave scattering producing strong spurious radiation exceeding the electron cyclotron emission (ECE) level by several orders of magnitude [2] - [6] and complicating the performance of the microwave plasma diagnostics [5], ion acceleration in the ECRH experiment when energy exchange between electrons and ions should be very low [7] - [9], significant broadening of the ECRH power deposition profile [10], [11]) were discovered in the ECRH experiments at different toroidal devices. They were interpreted as a consequence of low-power-threshold absolute parametric decay instabilities excited in the presence of a non-monotonic (hollow) density profile often encountered in existing fusion devices. The developed theory of the low-threshold PDI not only described the known anomalous effects but also predicted the gyrotron subharmonic emission during the ECRH experiments [12], that was confirmed in the experiment later [4]. The most dangerous scenario discovered in [13] is a PDI leading to excitation of two upper hybrid (UH) daughter waves trapped along the direction of the plasma inhomogeneity and localized on a magnetic

DOI: 10.1063/5.0132560

surface due to the finite pump width. In the case of inhomogeneous plasmas with monotonic background profiles, thresholds for different scenarios of parametric pump wave decay have been analyzed and evaluated by different authors more than three decades ago. The results of these studies, summarized e.g. in [14], predict power thresholds of the instability which are much higher than the power of modern gyrotrons. This is due to the huge convective energy loss of the daughter waves from the decay layer, which makes it impossible to amplify them significantly and makes one conclude that the pump wave is stable at EC heating. Meanwhile, if one or both daughter waves are somehow trapped in the decay region, this suppresses their energy loss and decreases the instability threshold. For a non-monotonic density profile, it becomes possible to localize the daughter wave/waves within the decay layer, thus reducing the instability threshold. In the last decade, various microwave decay scenarios have been analyzed. The results of this analysis, summarized in [15], predict the instability threshold at a level that is two orders of magnitude lower than that for a monotonic density profile.

The general scenario of the low-threshold PDI, leading to the excitation of a trapped UH wave and a running UH (or X-mode) wave, and its saturation were analyzed analytically in [15] - [17] and numerically in [18], [19] for various regimes of the instability assuming smooth Gaussian shape of the pump beam. However the analysis of the microwave beam propagation in plasma demonstrated that the beam characteristics can be significantly changed in the edge turbulent layer [20] - [24]. The beam distortion results in the average angular and spatial beam broadening, whereas a single random beam distribution may be split into several sub-beams. That leads to the question if the PDI theory, developed for the smooth pumping waves, still describes the instability characteristics well and how significant the difference can be for different scenarios of the edge plasma turbulence.

In the present paper the low-threshold two-UH-plasmon PDI and its saturation are investigated numerically for the pump wave beam distribution corrupted by the edge plasma turbulence. The key characteristics of the instability are evaluated and statistically analyzed. It is shown that the average PDI growth rate is reduced and the excitation threshold is increased, whereas the average instability saturation level and the anomalous energy absorption rate at the pump power substantially exceeding the threshold are almost independent on the plasma edge turbulence.

2 Description of the PDI model

First of all analytical description of the PDI process is provided in this section. The analysed instability model is the 2-step parametric decay of the pump under the conditions for which only one UH wave is trapped [15] - [17]. This decay, resulting in only one trapped plasmon, corresponds to the experimental conditions of the TEXTOR tokamak ECRH experiment at high and low densities [2],[3]. Normally a low-threshold parametric decay occurs in a small volume within which the decay conditions (conditions of the three-wave interaction resonance) are satisfied. This allows using the Cartesian coordinate system: x axis is a direction of inhomogeneity of the plasma density $n = n(x)$ which is typically associated with the radial coordinate, z axis is a direction of the external magnetic field $\mathbf{B}$ that is assumed to be perpendicular to x, and finally the y coordinate is the axes perpendicular to x and z and associated with the poloidal coordinated of a tokamak (see figure 1). We consider a monochromatic extraordinary pumping wave

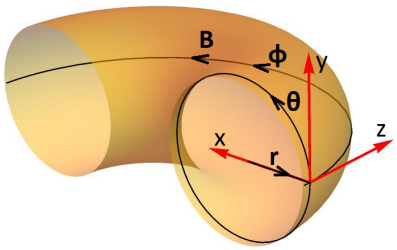

Figure 1: A tokamak (torus) transection, the external magnetic field $\mathbf{B}$ (its dominant toroidal part), the toroidal coordinates (r, θ, Φ) where $\mathbf{r}$ is the radius unit vector, $\mathbf{\Theta}$ and $\mathbf{\Phi}$ are the poloidal and toroidal unit vectors; the introduced Cartesian coordinates in red (x, y, z)

(X-mode) propagating along the radial coordinate x

$$\mathbf{E}_0 = \mathbf{e}_0 \sqrt{\frac{\omega_0}{ck_0(x)}} \frac{C_0(\mathbf{r})}{2} e^{-i\omega_0 t + i\int^x k_0(x')dx'} + c.c. \tag{1}$$

where the polarization vector $\mathbf{e}_0 = \frac{\mathbf{e}_y - i\frac{g_0}{\varepsilon_0}\mathbf{e}_x}{\left|\mathbf{e}_y - i\frac{g_0}{\varepsilon_0}\mathbf{e}_x\right|}$, $\mathbf{e}_{x,y}$ are the unit vectors along the corresponding coordinates, $\varepsilon(\omega) = 1 - \frac{\omega_{pe}^2}{\omega^2 - \omega_{ce}^2}$ and $g(\omega) = \frac{\omega_{ce}}{\omega}\frac{\omega_{pe}^2}{\omega^2 - \omega_{ce}^2}$ are components of the «cold» dielectric tensor so $\varepsilon_0 = \varepsilon(\omega_0)$ and $g_0 = g(\omega_0)$ (one should not be confused, ε_0 is not the vacuum electric permittivity constant here), where ω_{ce} and ω_{pe} are the electron-cyclotron and plasma frequencies; $k_0 = \frac{\omega_0}{c}\sqrt{\frac{\varepsilon_0^2 - g_0^2}{\varepsilon_0}}$ is the X-mode wave number, C_0 is the pump amplitude and c.c. stands for the complex conjugated part.

We consider a two-step decay of the extraordinary pump wave (1). In the first step, the pump wave experiences a primary decay into a trapped UH wave and a running UH wave, the UH waves can be described in terms of their potentials, the expressions for the trapped UH wave φ_m and the non-trapped one φ_b are

$$\begin{aligned} \varphi_m &= \frac{C_m(y,z,t)}{2}\psi_m(x)\, e^{-i\omega_m t} + c.c. \\ \varphi_b &= \frac{C_b(\mathbf{r},t)}{2} e^{i(\omega_0-\omega_m)t + i\int^x q_x^-(x',\omega_0-\omega_m)dx'} + c.c. \end{aligned} \tag{2}$$

$C_{m,b}$ are the amplitudes of the two waves, frequency of the trapped wave is ω_m, $q_x^{\pm}(x,\omega)$ are two roots of the UH waves dispersion equation

$$D_{UH}(q_x, \omega; x) = \frac{3}{2}\frac{\omega_{pe}^2}{\omega^2 - \omega_{ce}^2}\frac{v_{te}^2}{4\omega_{ce}^2 - \omega^2} q_x^4 + \varepsilon q_x^2 + \frac{\omega^2}{c^2} g^2 + \eta q_z^2 = 0 \tag{3}$$

describing the slow and fast modes with $q_y = 0$ and $q_z = 0$. In the equation (3) $v_{te} = \sqrt{\frac{2T_e}{m_e}}$ is the electron thermal velocity, the electron temperature T_e and mass m_e, $\eta = 1 - \frac{\omega_{pe}^2}{\omega^2}$, $q_{x,z}$ are the wave number components, the first term in (3) is the thermal amendment

to the cold plasma model, that is needed to describe the vicinity of the UH resonance. Since one wave is trapped the Bohr–Sommerfeld quantization condition must be fulfilled

$$\int_{x_l}^{x_r} dx' \left(q_x^+ \left(x', \omega_m \right) - q_x^- \left(x', \omega_m \right) \right) = 2\pi \left(m + \frac{1}{2} \right) \tag{4}$$

$x_{l,r}$ are the two turning points $q_x^- \left(x_{l,r}, \omega_m \right) = q_x^+ \left(x_{l,r}, \omega_m \right)$, $\psi_m \left(x \right)$ is the corresponding eigenfunction for the mode number m and represented by means of the WKB approximation as follows

$$\psi_m \left(x \right) = L_m^+ \left(x \right)^{-1/2} e^{i \int_{x_l}^x dx' q_x^+ \left(x', \omega_m \right) - i \frac{\pi}{4}} + L_m^- \left(x \right)^{-1/2} e^{-i \int_{x_l}^x dx' q_x^- \left(x', \omega_m \right) + i \frac{\pi}{4}} \tag{5}$$

where $L_m^\pm = \left| D_{qm}^\pm \right| \int_{x_l}^{x_r} dx' \left(\left| D_{qm}^+ \right|^{-1} + \left| D_{qm}^- \right|^{-1} \right)$ and $D_{qm}^\pm = \frac{\partial D_{UH}}{\partial q} \Big|_{q^\pm (x, \omega_m)}$ [17]. The primary decay takes place nearby the point where the decay resonance conditions for the wave numbers and frequencies are fulfilled

$$\begin{aligned} &\omega_m = \omega_0 - \left(\omega_0 - \omega_m \right) \\ &q_x^- \left(\omega_m \right) = k_0 + q_x^- \left(\omega_0 - \omega_m \right) \Big|_{x_d} \end{aligned} \tag{6}$$

where x_d is the decay point coordinate.

The trapped UH wave, when its amplitude $C_m \left(y, z, t \right)$ during the primary instability becomes large enough to overcome the secondary instability threshold, decays into a trapped UH wave φ_n and a running ion Bernstein (IB) wave

$$\begin{aligned} \varphi_n &= \frac{C_n \left(y, z, t \right)}{2} \psi_n \left(x \right) e^{-i \omega_n t} + c.c. \\ \varphi_I &= \frac{C_I \left(x, t \right)}{\sqrt{\left| \partial D_{IB} / \partial q_{Ix} \right|}} e^{-i \omega_I t + i \int^x dx' q_{Ix} (x')} + c.c. \end{aligned} \tag{7}$$

where C_n - the amplitude of the secondary trapped UH mode n, ψ_n is the corresponding eigenfunction defined by the equation (5), C_I is the IB wave amplitude, $\omega_I = \omega_m - \omega_n$, q_{Ix} is the wave number - a solution of the local dispersion equation $D_{IB} = \mathbf{q}^2 + \chi_e + \chi_i = 0$, where χ_e and χ_i are the electron and ion plasma susceptibilities, their explicit expressions can be found in many classical books on the plasma electrodynamics, in particular in [25]. The secondary decay occurs in the vicinity of the point x_s where the decay conditions are satisfied

$$\begin{aligned} &\omega_n = \omega_m - \omega_I \\ &q_x^- \left(\omega_n \right) = q_{Ix} - q_x^- \left(\omega_m \right) \Big|_{x_s} \end{aligned} \tag{8}$$

In this case of a two-step cascade decay of the pump wave (1), its depletion is negligible [15]. This allows omitting the equation describing the pump wave and considering its amplitude to be constant along the direction of its propagation - x coordinate. Then the

set of equations describing the two-step cascade decay reads

$$\int \frac{\mathbf{dq}dr'}{(2\pi)^3} D_{UH}\left(\mathbf{q},\omega_m,\frac{\mathbf{r}+\mathbf{r}'}{2}\right) e^{i\mathbf{q}(\mathbf{r}-\mathbf{r}')}\varphi_m(\mathbf{r}') = -\frac{1}{B}\hat{\chi}^a_{nl}\left((\mathbf{E}_0\mathbf{e}_x)\,\varphi_b\right) - \frac{|e|}{T_e}\hat{\chi}^b_{nl}\left(\varphi_I\varphi^*_n\right)$$
$$\int \frac{\mathbf{dq}dr'}{(2\pi)^3} D_{UH}\left(\mathbf{q},\omega_0-\omega_m,\frac{\mathbf{r}+\mathbf{r}'}{2}\right) e^{i\mathbf{q}(\mathbf{r}-\mathbf{r}')}\varphi_b(\mathbf{r}') = -\frac{1}{B}\hat{\chi}^a_{nl}\left((\mathbf{E}^*_0\mathbf{e}_x)\,\varphi_m\right)$$
$$\int \frac{\mathbf{dq}dr'}{(2\pi)^3} D_{UH}\left(\mathbf{q},\omega_n,\frac{\mathbf{r}+\mathbf{r}'}{2}\right) e^{i\mathbf{q}(\mathbf{r}-\mathbf{r}')}\varphi_n(\mathbf{r}') = -\frac{|e|}{T_e}\hat{\chi}^b_{nl}\left(\varphi_I\varphi^*_m\right)$$
$$\int \frac{\mathbf{dq}dr'}{(2\pi)^3} D_{IB}\left(\mathbf{q},\omega_I,\frac{\mathbf{r}+\mathbf{r}'}{2}\right) e^{i\mathbf{q}(\mathbf{r}-\mathbf{r}')}\varphi_I(\mathbf{r}') = -\frac{|e|}{T_e}\hat{\chi}^b_{nl}\left(\varphi_m\varphi_n\right) \tag{9}$$

where $\hat{\chi}^a_{nl}$ is a second-order differential operator over the x-coordinate, describing the coupling efficiency of the extraordinary wave with two electrostatic waves, $\hat{\chi}^b_{nl}$ is a fourth-order differential operator on the x-coordinate describing the coupling efficiency of three electrostatic waves. In the Fourier representation $\hat{\chi}^a_{nl}$ and $\hat{\chi}^b_{nl}$ are the familiar nonlinear plasma susceptibilities, the explicit expression of which can be found in [26]. The system (9) can be reduced to a system of two non-linear equations, the running wave amplitudes φ_b and φ_I can be expressed in terms of the trapped waves φ_n, φ_m and the pump E_0 amplitudes explicitly. To demonstrate this we solve the last equation in (9) in the WKB approach, the IB wave amplitude C_I obeys the following ODE

$$i\frac{\partial D_{IB}}{\partial q_{Ix}}\frac{e^{i\int^x dx' q_{Ix}(x')}}{\sqrt{|\partial D_{IB}/\partial q_{Ix}|}}\frac{\partial C_I}{\partial x} = -\frac{|e|}{T_e}\hat{\chi}^b_{nl}\left(\varphi_m\varphi_n\right) \tag{10}$$

Integrating this equation with the appropriate boundary condition $C_I\big|_{x\to-\infty} \to 0$ we arrive at

$$\varphi_I = i\frac{|e|}{T_e}\frac{e^{-i\omega_I t}}{\sqrt{|\partial D_{IB}/\partial q_{Ix}|}}\Big|_{x_d}\int_{-\infty}^{x} dx'\frac{e^{i\int_{x'}^{x} dx'' q_{Ix}(x'')}}{\sqrt{\partial D_{IB}/\partial q_{Ix}}}\hat{\chi}^b_{nl}\left(\varphi_m\varphi_n\right) + c.c. \tag{11}$$

We assume here that the secondary instability growth rate is much smaller than the IB wave frequency and moreover, much smaller than the ion cyclotron frequency. This assumption, which is valid for parameters of the present day tokamak experiments, allows correct consideration of both the instability saturation phase and the stage of its exponential growth. The IB wave amplitude (11) depends on the coordinates y, z and time t parametrically through the dependence of the UH m and n modes amplitudes on them. Thus the IB wave can be excluded from the whole system describing the two-step decay cascade, an analogous procedure can be applied for the non-trapped UH wave described by the potential φ_b. Then substituting the IB wave and the non-trapped UH wave potentials into the equations describing the primary and the secondary trapped UH waves, assuming a small pumping wave depletion, results in the set of the non-linear equations

$$\frac{\partial}{\partial t}a_m - i\Lambda_{my}\frac{\partial^2}{\partial y^2}a_m - i\Lambda_{mz}\frac{\partial^2}{\partial z^2}a_m = \gamma_p A(y,z)\,a_m - \gamma_s|a_n|^2 a_m$$
$$\frac{\partial}{\partial t}a_n + i\Lambda_{ny}\frac{\partial^2}{\partial y^2}a_n + i\Lambda_{nz}\frac{\partial^2}{\partial z^2}a_n = \gamma_s|a_m|^2 a_n \tag{12}$$

where the normalized amplitudes of the first trapped UH wave (m) and the secondary one (n) $a_{n,m} = C_{n,m}\sqrt{\frac{\omega\partial D_{UH}/\partial\omega\rho_z^2}{16\pi}}\Big|_{\omega=\omega_{n,m}}$, the amplitudes are normalized so that $|a_{n,m}|^2$ being multiplied by $\frac{T_e}{\pi\rho_z^2}$ gives the 2D energy density of the trapped plasmons, the energy of the plasmons $\epsilon_m = \frac{T_e}{\pi\rho_z^2}\iint dydz\,|a_m|^2$; the values $\Lambda_{my,mz} = \frac{\partial^2 D_{UH}}{2\partial q_{y,z}^2}\Big|_{\omega_m,q_{y,z}=0}$ have the meaning of the diffraction coefficients for the UH waves, the function $A(y,z)$ describes the spatial distribution of the pump beam intensity, which is calculated accounting for the edge plasma turbulence, the coefficient $\gamma_p \propto P_0/\rho_y\rho_z$ describes the nonlinear coupling between the waves participating in the primary decay, $\gamma_s \propto 1/\rho_z^2$ is the coefficient describing the interaction between the primary trapped UH wave, the secondary one and the IB wave, which is calculated with the due account of the thermal effects [26]. The explicit description for these coefficients and the derivation of the expressions (12) itself is quite bulky, now we are focused on the analysis of the system (12), for the details we refer the readers to [15], [17]. Dependence of these coefficients on the pump power and the beam radius is analyzed in [27]. The system (12) describes the UH waves evolution averaged within the volume of one plasmon trapping so the diffraction of the pump beam is neglected in this volume.

Normally the analytical and numerical investigation of the PDI processes are fulfilled in the model with a non-perturbed Gaussian pump beam distribution, i.e. the square of the pump wave amplitude modulus, being represented as follows

$$A^G(y,z) = e^{-\frac{y^2}{\rho_y^2}-\frac{z^2}{\rho_z^2}} \tag{13}$$

where the poloidal and toroidal beam widths $\rho_{y,z}$, and typically $\rho_y = \rho_z$. This standard pump beam shape will be used in the following analysis of (12). First of all the system (12) describes the exponential growth of the primary UH wave (the growth rate of the instability) and its saturation. The nonlinear term in the right-hand side of the first equation in (12) is negligible at the instability excitation stage. The solution of the corresponding linear equation is represented in terms of superposition of its 2D eigenfunctions, possessing its own growth rate. For the fundamental mode, characterised by the maximal growth rate Γ, well above the threshold we get the instability growth rate (see [16],[17])

$$\Gamma = Re(\gamma_p) - \cos\left(\frac{\arg(\gamma_p)}{2} - \frac{\pi}{4}\right)\sqrt{|\gamma_p|}\left(\sqrt{\frac{\Lambda_{my}}{\rho_y^2}} + \sqrt{\frac{\Lambda_{mz}}{\rho_z^2}}\right) \tag{14}$$

which is decreasing with widening of the pump beam in y and z directions. By putting $\Gamma = 0$ and recalling $\gamma_p \propto P_0/\rho_y\rho_z$ we can use the expression (14) also to estimate the instability excitation power threshold $P_0^{th} \propto \rho_y\rho_z\left(\sqrt{\frac{\Lambda_{my}}{\rho_y^2}} + \sqrt{\frac{\Lambda_{mz}}{\rho_z^2}}\right)^2$.

The second expression in the system (12) provides an estimate of the primary UH wave saturation amplitude. The saturation is determined by the balance between the secondary plasmon excitation source and its diffractive loss from the spot of the pump beam. So the estimate of the saturation amplitude provides the following expression:

$$\left|a_m^{sat}\right|^2 \approx \max\left\{\frac{\Lambda_{ny}}{\rho_y^2}, \frac{\Lambda_{nz}}{\rho_z^2}\right\}\frac{1}{\gamma_s} \tag{15}$$

normally $\Lambda_{nz} \gg \Lambda_{ny}$ so $|a_m^{sat}|^2 \propto 1$. The saturation of the secondary trapped UH wave is defined by the energy loss of the primary one

$$\left|a_n^{sat}\right|^2 \approx \frac{\gamma_p}{\gamma_s} \propto \frac{\rho_z}{\rho_y} \tag{16}$$

The pump beam loses some part of its initial power ΔP_0 due to the energy transfer to the daughter waves, this power does not serve to the purposes of the ECRH at the prescribed localization, thus the anomalous power absorption rate $\frac{\Delta P_0}{P_0}$ is an important characteristics. In the considered model the anomalous power absorption rate is given by the expression

$$\frac{\Delta P_0}{P_0} \approx \frac{2\omega_0}{\omega_m}\frac{T_e}{P_0}\gamma_p\frac{\rho_y}{\rho_z}\left|a_m^{sat}\right|^2 \propto 1/\rho_z^2 \tag{17}$$

see [28]. The system (12) is universal to describe the decay of an X-mode wave as well as an O-mode wave for the considered mechanism of the two-step cascade of the parametric decay. So the expression (17), derived in [28] for the O-mode pump, is applicable for the X-mode. The expression (17) provides an analytical value of the absorbed power ΔP_0, the numerical evaluation of this characteristic can be defined as the total energy increase of the primary and secondary trapped UH waves per a time unit

$$\Delta P_0 = \frac{d}{dt}\left(\epsilon_m + \epsilon_n\right) \tag{18}$$

All the described characteristics of the PDI process are possible to analyse analytically in the case of the Gaussian non-perturbed pumping beam profile. If the probing beam distribution A is a random function, corresponding to a random turbulence realization, numerical analysis of the system (12) is required to evaluate the PDI characteristics. The numerical solution of (12) in various turbulence regimes is analysed in the next section.

3 Pump beam distribution in turbulent plasma

3.1 Analytical description

The edge plasma turbulence can significantly distort the pump microwave beam [20] - [24]. If the turbulence amplitude is high enough, the radiation pattern can be split into several sub-beams whereas the average distribution of the electromagnetic field has the Gaussian shape. The results of the average beam structure analysis are described in this section, the turbulence parameters used to study the average beam widening influence on the PDI properties are defined.

The turbulence structure is strongly elongated along the magnetic field direction normally so the electron density turbulence δn is considered as a function of the radial and poloidal coordinates, in our geometry model $\delta n = \delta n\left(x, y\right)$. We consider an X-mode pumping microwave beam propagating in such turbulent plasma along the direction of the plasma inhomogeneity x. The wave structure at the plasma edge

$$E\left(x = 0, y, z\right) = E_0 e^{-\frac{y^2}{2\rho_0^2} - \frac{z^2}{2\rho_0^2}} \tag{19}$$

ρ_0 is the initial beam width and E_0 is the beam amplitude at the plasma edge. Since the turbulence is independent on z coordinate the beam width broadening in this direction is determined only by the diffraction. The analysis of the average field intensity was performed for the X-mode in [24] in the 2D model, the generalization of that analysis to 3D geometry (taking into account the beam structure in the toroidal direction z) results in the following expression for the average radiation intensity

$$\left\langle \left|\mathbf{E}\left(x,y,z\right)\right|^2\right\rangle = E_0^2 \frac{\omega_0}{ck_0\left(x\right)} \frac{\rho_0^2}{\rho_y\left(x\right)\rho_z\left(x\right)} e^{-\frac{y^2}{\rho_y^2(x)}} e^{-\frac{z^2}{\rho_z^2(x)}} \tag{20}$$

the poloidal and toroidal beam width components

$$\begin{aligned} \rho_y^2\left(x\right) &= \rho_0^2 + \frac{d_y^4\left(x\right)}{\rho_0^2} + \frac{1}{\pi}\int_{-\infty}^{\infty} dq_y \left|\delta n_{0,q_y}\right|^2 q_y^2 \int_0^x dx' \kappa^2(x') \frac{\delta\tilde{n}^2(x')}{n^2\left(x'\right)} \left(d_y^2\left(x\right) - d_y^2\left(x'\right)\right)^2 \\ \rho_z^2\left(x\right) &= \rho_0^2 + \frac{d_z^4\left(x\right)}{\rho_0^2} \end{aligned} \tag{21}$$

where $\kappa(x) = \frac{1}{k_0(x)} \frac{\omega_{pe}^2}{2c^2} \frac{\left(\omega_0^2-\omega_{ce}^2\right)\left(\omega_0^2-2\omega_{pe}^2\right)+\omega_{pe}^4}{\left(\omega_0^2-\omega_{ce}^2-\omega_{pe}^2\right)^2}$, d_y^2 and d_z^2 describe the diffraction of the beam in the two directions, $d_y^2(x) = \int_0^x dx' \frac{1}{k_0(x')}$ and $d_z^2(x) \approx d_y^2(x)$; the relative turbulence amplitude $\frac{\delta\tilde{n}^2(x)}{n^2(x)}$ and the turbulence spectrum $\left|\delta n_{q_x,q_y}\right|^2 = \int d\Delta x d\Delta y CCF\left(\Delta x,\Delta y\right) e^{-i\Delta x q_x - i\Delta y q_y}$ are defined according to the averaging procedure

$$\left\langle \frac{\delta n(x',y')}{n(x')} \frac{\delta n(x'',y'')}{n(x'')} \right\rangle = \frac{\delta\tilde{n}^2\left(\left(x'+x''\right)/2\right)}{n^2\left(\left(x'+x''\right)/2\right)} CCF\left(x'-x'',y'-y''\right) \tag{22}$$

The first term in the expression for ρ_y^2 (21) stands for the initial probing beam size squared, the second one represents diffraction, taking into account refractive index in inhomogeneous medium, the third part describes the effect of the beam broadening due to the plasma turbulence. The criterion for the applicability of this analysis is the big enough value of the average phase variation associated with the turbulence $<\delta\phi^2> \gg 1$. For the detailed description we refer the readers to [24].

3.2 Numerical modelling

A probing microwave beam poloidal distribution in turbulent plasma is simulated in this section. The 2D beam propagation is considered in the slab model, the x axis is the direction of the density $n\left(x\right)$ and magnetic field $B\left(x\right)$ inhomogeneity, the y axis represents poloidal direction, propagation in the toroidal direction z is not simulated since the turbulence is normally elongated in this direction and does not perturb ρ_z (21). The beam propagates along the direction of the inhomogeneity x, the probing frequency is $f = 82.4$ GHz, the initial beam width $\rho_0 = 1.0$ cm. The size of the numerical cells is $\lambda_0/24$ in the x and y directions with λ_0 being the vacuum wave number at the pump wave frequency, the 2D simulation domain is 1000×1000 cells, the time step is $\Delta t = 1/48f$, the full time of each simulation is $20000\Delta t$ which is enough for the pump wave pass through the simulation domain. The simulation is performed for the plasma conditions similar to the ECRH experiment at TCV, which will be used to the study

the impact of the turbulence on the PDI characteristics. The density and magnetic field profiles measured in the shot 41383 were used, figures 2 and 3 respectively, where $x = 0$ represent the vicinity of the last closed surface, the measured profiles were extrapolated to the region $x < 0$. The frozen turbulence, that is adequate for the high-frequency pump, was generated as a sum of spacial harmonics obeying the Gaussian spectrum and possessing random phases $\phi_{k,l}$, this is a standard approach often used for modeling the turbulence, that allows to control the turbulence parameters easily

$$\delta n\left(x,y\right)=\delta n^{rms}\left(x\right)\quad\frac{1}{2}\sum_{k,l}\exp\left[-\frac{1}{4}\left(q_k^2+q_l^2\right)l_c^2\right]\Bigg)^{-1/2}\times$$
$$\sum_{k,l}\exp\left[-\frac{1}{8}\left(q_k^2+q_l^2\right)l_c^2\right]\cos\left[q_kx+q_ly+\phi_{k,l}\right] \tag{23}$$

$q_{k,l}$ are the discrete wavenumbers, $\delta n^{rms}\left(x\right)$ is the root mean square value of the turbulence, $l_c = 0.5$ cm is the used correlation length. The turbulence amplitude Q is defined as $Q=\frac{\delta n^{rms}(0)}{n(0)}$. The shape of $\delta n^{rms}\left(x\right)$ is illustrated on the figure 2 (the dashed curve) for the turbulence amplitude $Q = 0.2$. It should be mentioned that the stationary turbulence model also implies that the characteristic time of the turbulence change is much higher than the reversed instability growth rate Γ^{-1}. This condition usually holds for the drift-wave edge plasma turbulence possessing correlation time of several microseconds. The simulations of the beam propagation in the turbulent plasma are performed by using the full-wave code IPF-FD3D.

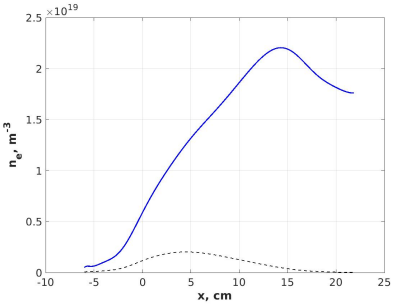

Figure 2: The profiles of the density $n\left(x\right)$ and the turbulence root mean square value $\delta n^{rms}\left(x\right)$ for the case of the amplitude $Q = 0.2$, the solid and dashed curves respectively

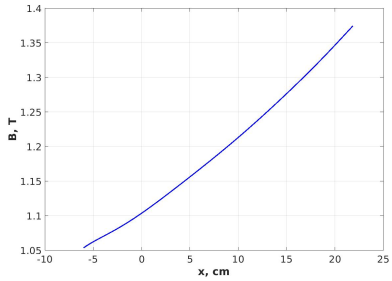

Figure 3: The magnetic field profile used in the simulation

The simulations were performed in the three turbulence regimes for the different turbulence amplitudes $Q = \{0.1, 0.2, 0.4\}$ and in the case without the turbulence $Q = 0$. The poloidal distribution of the pump beam intensity is evaluated around the position $x = 20$ cm, where the PDI takes place. The examples of the normalized distributions are illustrated on the figures 4 - 6 for the different turbulence amplitudes. It is seen that the injected beam can be significantly distorted by the edge turbulence, the relatively weak turbulence ($Q = 0.1$) perturbs the microwave beam, whereas the beam can be split into several smaller ones in the case of the high turbulence amplitude ($Q = 0.4$).

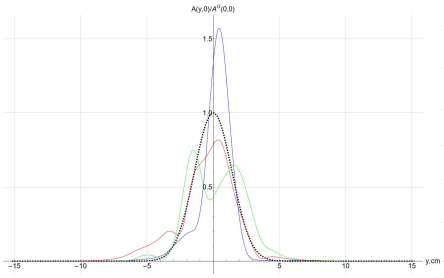

Figure 4: The normalized random poloidal profiles of the pump beam - the solid curves, the turbulence amplitude $Q = 0.1$; the dashed curve is the poloidal distribution in the case without the turbulence

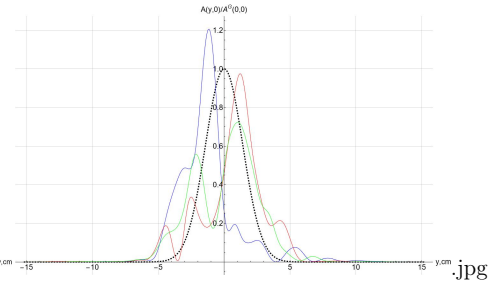

.jpg

Figure 5: The normalized random poloidal profiles of the pump beam - the solid curves, the turbulence amplitude $Q = 0.2$; the dashed curve is the poloidal distribution in the case without the turbulence

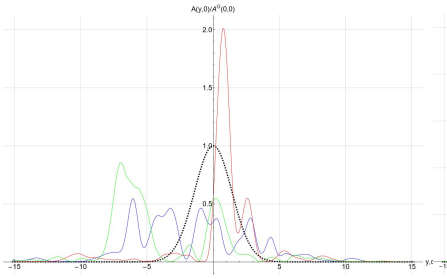

Figure 6: The normalized random poloidal profiles of the pump beam - the solid curves, the turbulence amplitude $Q = 0.4$; the dashed curve is the poloidal distribution in the case without the turbulence

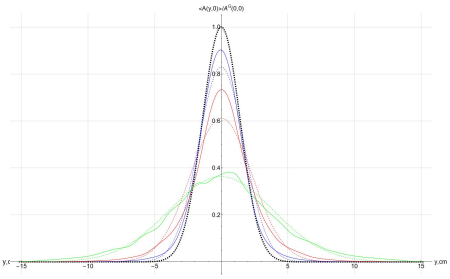

Figure 7: The solid curves are the average over 400 realizations poloidal profiles of the intensity, the blue, red and green colors correspond to the turbulence amplitudes $Q = \{0.1, 0.2, 0.4\}$ respectively, the dashed curves of the same colors are the analytical prediction of the nonlinear theory; the black dashed curve is the poloidal distribution in the case without the turbulence

The profiles of the normalized intensity averaged over 400 realizations are illustrated on the figure 7. The average numerically evaluated profiles are compared with the analytical prediction (20), (21) given by the dashed curves. For the relatively small turbulence amplitudes $Q = \{0.1, 0.2\}$ the pump phase modulation is not big enough $< \delta\phi^2 > \approx \{0.3, 1.4\}$ to guarantee the applicability of the analytical averaging procedures. This explains a non-perfect fit of a numerical computation averaging result by the analytical expression (20) for the pump beam seen in figure 7. The agreement is better in the case of the higher turbulence amplitude $Q = 0.4$ when $< \delta\phi^2 > \approx 5.6$. The average poloidal beam width evaluated using (21) is corresponding $\rho_y \approx \{2.0, 2.4, 3.3, 5.5\}$ cm for the four considered turbulence regimes $Q = \{0, 0.1, 0.2, 0.4\}$.

As it was mentioned the toroidal distribution of the beams $A(0, z)$ is not perturbed by the turbulence, its shape is Gaussian, the poloidal distribution $A(y, 0)$ was evaluated from the numerical modelling in the three turbulence scenarios $Q = \{0.1, 0.2, 0.4\}$, their combination describes the 2D spatial distribution of the pump beam. The 2D distribution is used in the system (12) for the evaluation of the PDI characteristics, the results are compared with the PDI characteristics in the case of the non-perturbed beam $A(y, z) = A^G(y, z)$.

4 The PDI numerical analysis

The parametric decay of a Gaussian microwave beam is described analytically in the first section, its characteristics can be expressed in terms of the beam width and power. The obtained results could be applied both to the case of unperturbed pump beam and to the case of the averaged beam (20). The PDI process in the turbulent plasma, when the heating radiation poloidal distribution is a random function, can be analysed numerically. The numerical solution of the system (12) in the different turbulence scenarios for the various turbulence amplitudes Q, described in the previous section, is analyzed in this section. The PDI characteristics averaged over a large set of independent turbulence realizations, having the same correlation lengths, spectrum and amplitude, are evaluated and compared against the results of the modeling without the turbulence.

The system (12) is solved with the coefficients typical for the ECRH experiments at TCV and with the initial condition of the thermal noise level amplitudes $a_{n,m} = 1$, the electron temperature $T_e = 2$ keV, the pump beam power $P_0 = 600$ kW and the width of the non-perturbed Gaussian beam $\rho = \rho_{y,z} = 2$ cm. The periodic boundary conditions were used, however the effect of the trapped UH waves multiple transitions through the parametric decay area, which is possible to model with these conditions, was not considered.

4.1 Growth rate and saturation

The growth rate of the instability is described by the stage of the exponential growth of the primary trapped UH wave amplitude. The wave energy averaged within the pump beam area $\epsilon_m^{av} = \frac{T_e}{\pi\rho_z^2} \iint dydz \left|a_m\right|^2 A\left(y,z\right)$ is convenient for the analysis of the growth rate and the saturation amplitude, the full energy ϵ_m grows with the time without the saturation. The statistically average function $\mathrm{Ln}\frac{\epsilon_m^{av}(t)}{\epsilon_m^{av}(0)}$ is depicted on the figure (8) for the four turbulence amplitudes $Q = \{0, 0.1, 0.2, 0.4\}$. The numerically evaluated energy evolution in the instability excitation stage is compared with the analytical prediction (14) for $2\Gamma t$, where the growth rate Γ is evaluated for the different average pump beam widths ρ_y, corresponding to the different turbulence regimes. The qualitative concordance between the theory prediction (14) and the numerical results for the averaged Gaussian pump beams is reasonable. The simulations demonstrate that the relatively small turbulence amplitudes $Q = \{0.1, 0.2\}$ almost do not change the average growth rate. The higher level of the turbulence $Q = 0.4$ reduces the average growth rate, but the analytical prediction for the averaged beam overestimates by a factor of 2 the effect of the growth rate decrease (see figure 8). A possible explanation for this is provided by the dependence of the growth rate not on the beam power or width, but on the pump electric field, which can be large in the disturbed beam. The saturation level of the primary plasmon energy located within the pump beam is fluctuating, however remaining almost the same for all the turbulence regimes. This result corresponds to the expression (15) since usually $\Lambda_{nz} \gg \Lambda_{ny}$ so that the saturation level is determined by the pump beam distribution along the magnetic field, not affected by the turbulence, and independent on the poloidal beam structure.

The energy evolution of the secondary trapped plasmon is illustrated on the figure 9. It is seen that the energy saturation level decreases with increasing the turbulence amplitude. This tendency can be explained if one considers the PDI process driven by

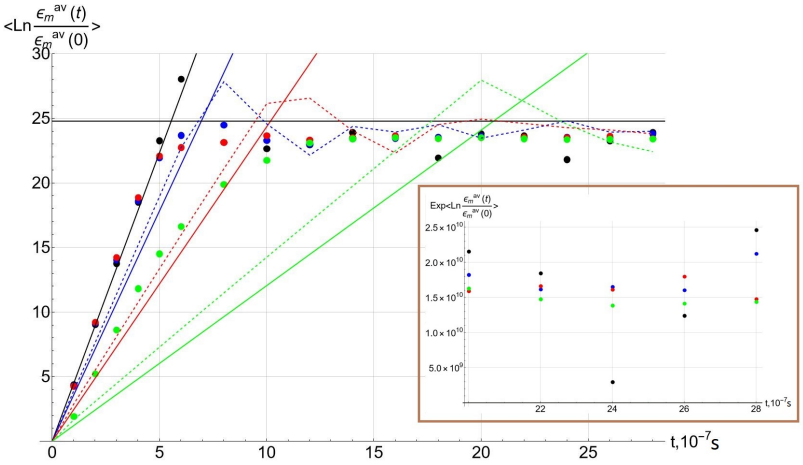

Figure 8: The primary trapped UH wave energy evolution $\left\langle \mathrm{Ln}\frac{\epsilon_m^{av}(t)}{\epsilon_m^{av}(0)} \right\rangle$, the black, blue, red and green dotted curves, provided by the numerical solution of (12), represent the case without the turbulence and the simulations with $Q = \{0.1, 0.2, 0.4\}$ respectively, the solid lines of the same colors provide the $2\Gamma t$ value, with the growth rate Γ evaluated using (14) for the different averaged beam widths, corresponding according to (21) to the turbulence amplitudes Q, the dashed curves are provided by the numerical solutions of (12) for the unperturbed Gaussian pump with the corresponding (the same color) average beam widths ρ_y, the horizontal line is the estimate of the saturation level for the non-perturbed pump beam; the saturation stage is depicted in the framed graphic in the linear scale

the averaged pump beam. Namely, according to the analytical estimate (16) $|a_n^{sat}|^2 \propto \rho_z/\rho_y$, the average poloidal beam width ρ_y is increasing due to the edge turbulence. The analytical estimates of the energy saturation level slightly overestimate the saturation values of $\epsilon_{m,n}^{av}$.

4.2 Anomalous absorbtion

The total energy of the primary and secondary trapped UH waves $\epsilon_m + \epsilon_n$ increase per second determines the amount of the anomalously absorbed pumping power according to the expression (18). The total energy evolution was evaluated and averaged in the saturation stage of the instability for the different turbulence regimes $Q = \{0, 0.1, 0.2, 0.4\}$, the results are depicted on the figure 10. As it is seen, the total energy can be approximated well by a linear function, the least mean squares fitting is illustrated on the figure 10. The linear approximation is used for evaluating the energy anomalous absorbtion rate $\frac{\Delta P_0}{P_0} \approx \{4.8, 4.3, 4.5, 4.3\} \times 10^{-4}$ for the different turbulence amplitudes correspondingly. It is seen that presence of the turbulence results in only a small (of about 10%) mitigation of the anomalously absorbed power. This result agrees with the analytical prediction (17) which provides the dependency $\Delta P_0 \propto 1/\rho_z^2$ (assuming that normally $\Lambda_z \gg \Lambda_y$) so the anomalously absorbed power is not related to the poloidal pump beam width ρ_y, that is why one could expect the independence of ΔP_0 on the turbulence level. The energy $\langle \epsilon_m + \epsilon_n \rangle$ evolution curve for the case with the unperturbed plasma density

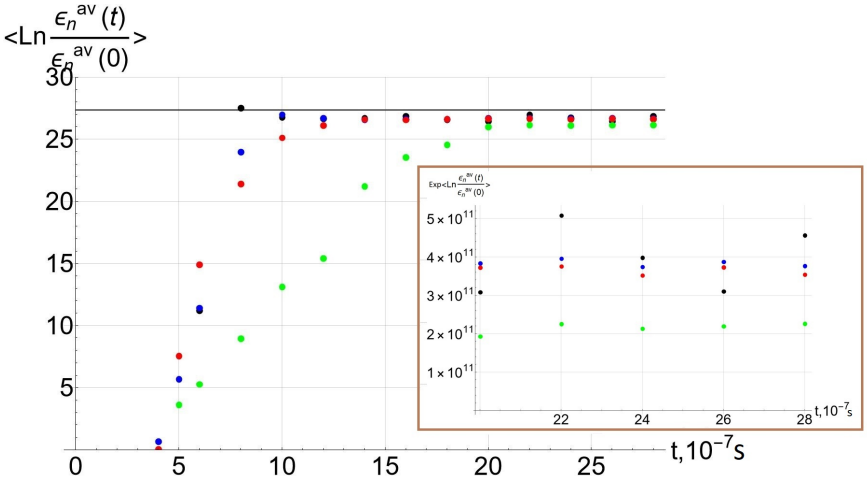

Figure 9: The secondary trapped UH wave energy evolution $\left\langle \mathrm{Ln}\frac{\epsilon_n^{av}(t)}{\epsilon_n^{av}(0)} \right\rangle$, the black, blue, red and green dotted curves represent the case without the turbulence and the simulations with $Q = \{0.1, 0.2, 0.4\}$ respectively, the horizontal line is the estimate of the saturation level for the non-perturbed beam; the saturation stage is depicted on the framed plot in the linear scale

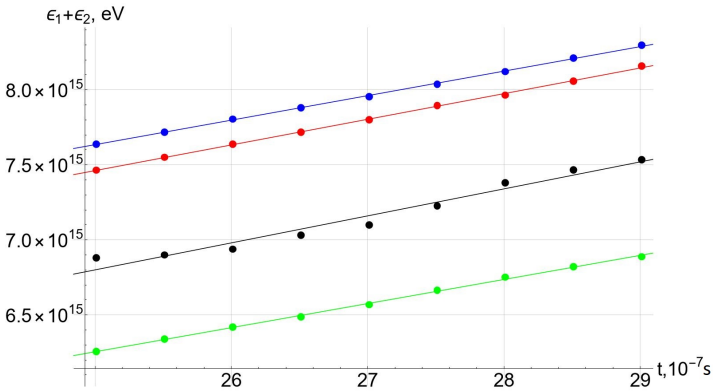

Figure 10: The total energy of the two trapped UH waves $\langle \epsilon_m + \epsilon_n \rangle$, the black, blue, red and green dotted curves represent the case without the turbulence and the simulations with $Q = \{0.1, 0.2, 0.4\}$ respectively; the solid lines of the same colors are the least mean squares fitting of the energy

is located between the curves corresponding to the high and low turbulence regimes in figure 10, this effect is due to the process of instability transition to the saturation, which is oscillatory. It has not got an analytical description yet.

4.3 Power threshold

The turbulence reduces the pump beam amplitude on average (figure 7), that leads to the increase of the instability threshold P_0^{th}. First of all it worth considering the threshold in the unperturbed beam case. According to the definition done in the first section the power threshold is determined from the relation $\Gamma = 0$, in the framework of the simulation model that results in $P_0^{th} \approx 47.1$ kW. The solution of the linearized first equation in the system (12) is illustrated on the figure 11 for the case without the plasma turbulence $Q = 0$. The solutions are obtained for the different power values P_0 in the range from $0.9P_0^{th}$ to $2.0P_0^{th}$. It is seen that the excitation does not occur when the pump power is lower than the threshold $P_0 = 0.9P_0^{th}$, if the power exceeds the threshold value, the energy evolution corresponds to the analytical prediction for its growth rate $Ln\left(|a_m(t)|^2 / |a_m(0)|^2\right) = 2\Gamma\left(P_0\right)t$. The evolution of the average local energy density $|a_m(t)|^2$ is depicted on the figures 12-14 for the simulations with the turbulence amplitudes $Q = \{0.1, 0.2, 0.4\}$ respectively. One can see that well above the threshold the

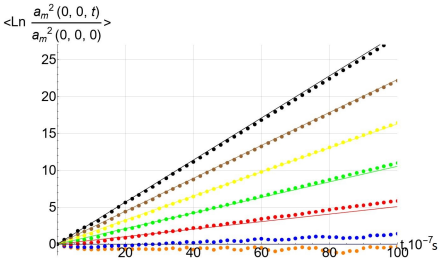

Figure 11: Evolution of $Ln\left(|a_m(t)|^2 / |a_m(0)|^2\right)$ evaluated in the point $(y = 0, z = 0)$ the case without the turbulence, the dotted orange, blue, red, green, yellow, brown and black curves are the numerical solutions for the power amplitudes $P_0 = 0.9, 1.0, 1.2, 1.4, 1.6, 1.8, 2.0\ P_0^{th}$ respectively, the solid lines are $2\Gamma t$ with the growth rate Γ evaluated for the corresponding power P_0

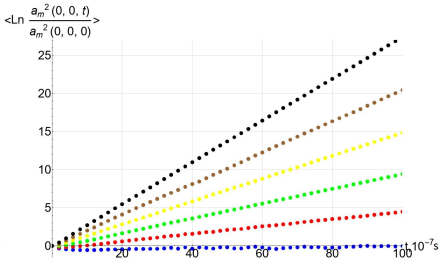

Figure 12: Evolution of $Ln\left(|a_m(t)|^2 / |a_m(0)|^2\right)$ evaluated in the point $(y = 0, z = 0)$ for the turbulence amplitude $Q = 0.1$, the dotted blue, red, green, yellow, brown and black curves are the numerical solutions for the power amplitudes $P_0 = 1.0, 1.2, 1.4, 1.6, 1.8, 2.0\ P_0^{th}$ respectively

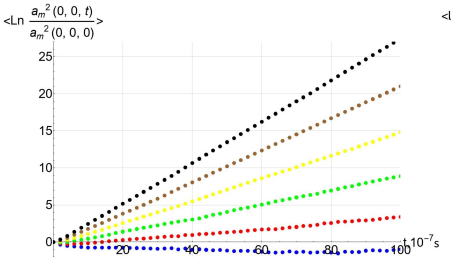

Figure 13: Evolution of $Ln\left(|a_m(t)|^2 / |a_m(0)|^2\right)$ evaluated in the point $(y = 0, z = 0)$ for the turbulence amplitude $Q = 0.2$, the dotted blue, red, green, yellow, brown and black curves are the numerical solutions for the power amplitudes $P_0 = 1.0, 1.2, 1.4, 1.6, 1.8, 2.0\ P_0^{th}$ respectively

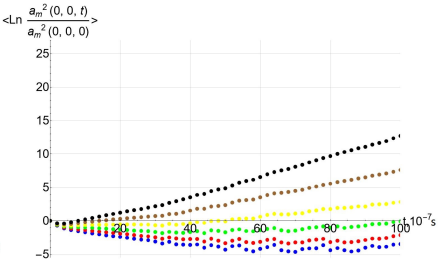

Figure 14: Evolution of $Ln\left(|a_m(t)|^2 / |a_m(0)|^2\right)$ evaluated in the point $(y = 0, z = 0)$ for the turbulence amplitude $Q = 0.4$, the dotted blue, red, green, yellow, brown and black curves are the numerical solutions for the power amplitudes $P_0 = 1.0, 1.2, 1.4, 1.6, 1.8, 2.0\ P_0^{th}$ respectively

presence of the low-level turbulence $Q = \{0.1, 0.2\}$ only slightly decreases the UH waves local energy density growth rate. The reliable exponential growth is observed on the

figures 12 and 13 even for the simulations with $P_0 = 1.2P_0^{th}$. The excitation threshold is noticeably higher in the simulation with the high turbulence amplitude $Q = 0.4$. The clearly exponential growth of the energy density starts since the power amplitude $P_0 = 1.6P_0^{th}$. The estimate of the average power threshold is illustrated on the figure 15, the estimated values are determined as the power for which the clear exponential growth is seen (the figures 12 - 14), whereas the error bar is provided by the range between the determined power threshold and the lower value of the power tested on the figures 12 - 14. The averaged power thresholds are compared to the threshold values for the Gaussian beams with the poloidal beam widths ρ_y corresponding to the averaged beam widths for the examined turbulence scenarios. The amplitudes of the evaluated power thresholds were defined in the same way as for the unperturbed Gaussian beam on the figure 11. It is seen from the figure 15 that if one considers the PDI process driven by

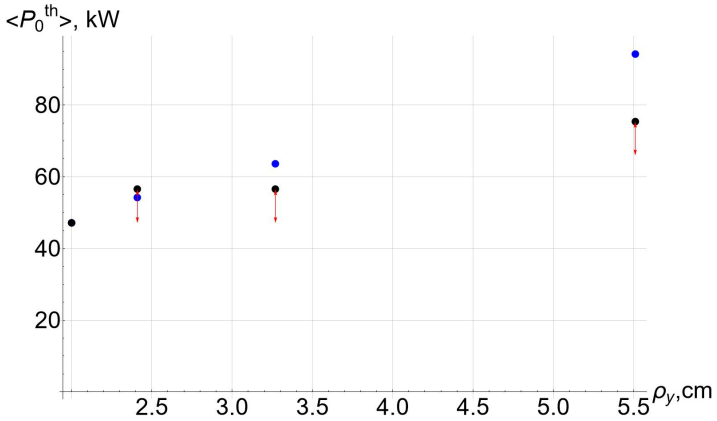

Figure 15: The average power threshold in the turbulent plasma is given by the black dots, the different ρ_y correspond to the different average beam widths in the considered turbulence regimes, the red arrows represent the error range of the threshold definition; the blue dots are the power threshold values for the Gaussian beams with the corresponding poloidal beam width.

a pump disturbed in a strongly turbulent plasma as a parametric decay of the averaged pump beam, the evaluated power threshold can be overestimated for about 20-30%.

5 Conclusion

The parametric decay instability in the turbulent plasma was simulated and analysed in this work under the plasma conditions close to the experimental ones on TCV tokamak. The tested turbulence regimes can be considered as the low turbulence $Q = 0.1$, ($\langle\delta\phi^2\rangle \ll 1$) the high turbulence $Q = 0.4$ ($\langle\delta\phi^2\rangle \gg 1$) and the intermediate turbulence ($\langle\delta\phi^2\rangle \approx 1$) scenarios. The investigated characteristics of the PDI process are the instability growth rate, its saturation level, the excitation threshold and the anomalous energy absorbtion rate. The simulations demonstrated that the instability growth rate in the small and intermediate turbulence regimes remains almost the same whereas the high-level turbulence slightly reduces the growth rate. The saturation level of the UH

wave energy density, averaged within the pump beam area, is independent on the turbulence amplitude for the primary trapped UH wave and decreased for the secondary trapped plasmon with growing the turbulence amplitude Q. The both tendencies are in agreement with the analytical predictions for the PDI considered in the field of the average pump beam. The average power threshold of the decay instability is just a little bit increased in the small and intermediate turbulence regimes whereas the threshold increase is about 50% for the high turbulence scenario. One of the most important in practice characteristics - the anomalous absorbtion rate is only slighted modified by the plasma turbulence. Its reduction constitutes only about 10% of the unperturbed value, and this mitigation remains the same for all the tested turbulence regimes.

In general, when the pump power is well above the threshold, the presence of the plasma turbulence does not modify the PDI characteristics drastically. The physical picture of a PDI process in the turbulent plasma is the nonlinear interaction of the waves (12), when the pump beam shape is slightly disturbed or even split into several sub-beams with their local peaks smaller or higher than the unperturbed beam amplitude and the different local sub-beam width. There is no analytical model that can describe the PDI characteristics in such a disturbed beam, one of the possible ways to predict the PDI characteristics in the case of the pump modulated by the edge plasma turbulence is to consider the parametric decay in the field of the average pump beam, however keeping in mind that the numerical study has demonstrated that this approach overestimates the turbulence influence on the PDI threshold and growth rate.

Acknowledgements
The PDI analytical and numerical treatment were supported under the RSF 22-12-00010 grant, the numerical modelling of the pump beam broadening was supported under the Ioffe Institute state contract 0040-2019-0023, whereas the code describing the PDI evolution and saturation was developed under the Ioffe Institute state contract 0034-2021-0003 The simulations of a beam propagation in the turbulent plasma were performed using the full-wave code IPF-FD3D provided by Dr. Carsten Lechte.

References

[1] B I Cohen, R H Cohen, W M Nevins, T D Rognlien 1991 *Rev. Mod. Phys.* **63** 949

[2] E Westerhof, S K Nielsen, J W Oosterbeek, M Salewski, M R De Baar, W A Bongers, A Bürger, B A Hennen, S B Korsholm, F Leipold, D Moseev, M Stejner, D J Thoen and the TEXTOR Team 2009 *Phys. Rev. Lett.* **103** 125001

[3] S K Nielsen, M Salewski, E Westerhof, W Bongers, S B Korsholm, F Leipold, J W Oosterbeek, D Moseev, M Stejner and the TEXTOR Team 2013 *Plasma Phys. and Control. Fusion* **55** 115003

[4] S K Hansen, S K Nielsen, J Stober, J Rasmussen, M Stejner, M Hoelzl, T Jensen and the ASDEX Upgrade team 2020 *Nucl. Fusion* **60** 106008

[5] S K Hansen, A S Jacobsen, M Willensdorfer, S K Nielsen, J Stober, K Höfler, M Maraschek, R Fischer, M Dunne, the EURO fusion MST team and the ASDEX Upgrade team, 2021 *Plasma Phys. Control. Fusion* **63** 095002

[6] A Tancetti, S K Nielsen, J Rasmussen, E Z Gusakov, A Yu Popov, D Moseev, T Stange, M G Senstius, C Killer, M Vecsei, T Jensen, M Zanini, I Abramovic, M Stejner, G Anda, D Dunai, S Zoletnik, H Laqua 2022 *Nucl. Fusion* **62** 074003

[7] S Coda and for the TCV Team 2015 *Nucl. Fusion* **55** 104004

[8] B Zurro, A Baciero, V Tribaldos, M Liniers, A Cappa, A Lopez-Fraguas, D Jimenez-Rey, J M Fontdecaba and O Nekhaieva 2013 *Nucl. Fusion* **53** 083017

[9] M Martínez, B Zurro, A Baciero, D Jimenez-Rey and V Tribaldos 2018 *Plasma Phys. Controlled Fusion* **60** 025024

[10] Yu N Dnestrovskij, A V Danilov, A Yu Dnestrovskij, S E Lysenko, A V Melnikov, A R Nemets, M R Nurgaliev, G F Subbotin, N A Solovev, D Yu Sychugov and S V Cherkasov 2021 *Plasma Phys. Control. Fusion* **63** 055012

[11] A I Meshcheryakov, I Yu Vafin and I A Grishina 2020 *Plasma Phys. Rep.* **46** 1144

[12] E Z Gusakov, A Yu Popov and P V Tretinnikov 2019 *Nucl. Fusion* **59** 106040

[13] A Yu Popov, E Z Gusakov 2015 *Plasma Phys. Control. Fusion* **57** 025022

[14] B I Cohen, R H Cohen, W M Nevins, T D Rognlien 1991 *Rev. Mod. Phys.* **63** p. 949

[15] E Z Gusakov, A Yu Popov 2020 *Phys. Usp.* **63** 365

[16] A Yu Popov, E Z Gusakov 2016 *Europhys. Lett.* **116** 45002

[17] E Z Gusakov, A Yu Popov, A N Saveliev 2018 *Physics of Plasmas* **25** 062106

[18] M G Senstius, S K Nielsen and R G L Vann 2021 *Plasma Phys. Control. Fusion* **63** 065018

[19] M G Senstius, E Z Gusakov, A Yu Popov, S K Nielsen 2022 *Plasma Phys. Control. Fusion* **64** 115001

[20] E V Sysoeva, F da Silva, E Z Gusakov, S Heuraux, A Yu Popov 2015 *Nucl. Fusion* **55(3)** 033016

[21] N Bertelli, G J Kramer and E J Valeo 2019 *Plasma Phys. Control. Fusion* **61** 105018

[22] A Snicker, E Poli, O Maj, L Guidi, A Köhn, H Weber, G D Conway, M Henderson and G Saibene 2018 *Plasma Phys. Control. Fusion* **60** 014020

[23] M W Brookman, M E Austin, C C Petty, R J La Haye, K Barada, T L Rhodes, Z Yan, A Kohn, M B Thomas, J Leddy, and R G L Vann 2021 *Phys. Plasmas* **28** 042507

[24] P V Tretinnikov, E Z Gusakov and S Heuraux 2021 *Plasma Phys. and Control. Fusion* **63** 085003

[25] A I Akhiezer, I A Akhiezer, R V Polovin, A G Sitenko, K N Stepanov "Plasma Electrodynamics" Volume 1 1975

[26] E Z Gusakov and A Yu Popov and P V Tretinnikov 2019 *Plasma Phys. Control. Fusion* **61** 085008

[27] E Z Gusakov and A Yu Popov 2022 *Plasma Physics Reports* **48** 327–336

[28] E Z Gusakov and A Yu Popov 2021 *Plasma Phys. Control. Fusion* **63** 015016